J. Fluid Mech. (1985), *vol.* 157, *pp.* 501–518
Printed in Great Britain

A linear analysis of rotating stratified flow past a circular cylinder on an f-plane

By LEE-OR MERKINE

Department of Mathematics, Technion – Israel Institute of Technology, Haifa 32000, Israel

(Received 17 July 1984 and in revised form 20 March 1985)

A linear analysis of rotating stratified flow past a circular cylinder on an f-plane is made for moderate and strong stratification, i.e. for $\sigma S = O(E^{\frac{1}{2}})$ and $\sigma S = O(1)$ respectively. E is the Ekman number and σS is the product of the Prandtl number and the inverse rotational Froude number. The most striking result is that, for oncoming flows that are of one sign and possess vertical shear, reversed-flow regions can exist next to the cylinder. Depending on the degree of stratification, these backflow regions can occupy the inner part of the vertical boundary layer or can extend horizontally across distances comparable to the horizontal scale of the cylinder.

1. Introduction

Boyer (1970) pioneered the study of flow separation in rotating systems by carrying out a series of experiments describing slightly viscous homogeneous flow past a circular cylinder in a rapidly rotating system. The cylinder extended throughout the depth of the fluid, its axis parallel to the constant rotation vector. The experiments showed that in the limit of zero Rossby number the flow was fully attached. However, for small but finite Rossby numbers separation occurred. The experiments showed also the emergence of asymmetry of the flow pattern with respect to the upstream flow direction, and it became more pronounced for successively larger Rossby numbers.

Using the quasi-geostrophic approximation, Walker & Stewartson (1972) derived a criterion for flow separation which is expressed as a ratio of the Rossby number to the square root of the Ekman number. However, their analysis could not explain the observed asymmetry. Merkine & Solan (1979) reconsidered the problem and suggested a mechanism for the asymmetry, which is based on incorporating higher-order Rossby-number effects. Their criterion for separation was identical with that of Walker & Stewartson.

Additional and more refined experiments were conducted by Boyer & Davies (1982), who emphasized beta-plane effects. Their results generally conformed with the earlier predictions of Merkine (1980) that beta inhibits separation for prograde flows.

The dynamics of the atmosphere and oceans is stratified and it is influenced by baroclinic effects. Hence it is important to understand the dynamics of vertical rotating stratified boundary layers. The simplest way of incorporating stratification into the dynamics is by considering the physically realizable two-layer model, an approach recently taken by Brevdo & Merkine (1985). The dynamics of each layer is fundamentally homogeneous, but the two layers are coupled through the frictional interface. This coupling is sufficient for altering qualitatively the response of the

system. The Taylor–Proudman constraint is broken by the stratification, which is concentrated at the interface, and this permits flows with vertical shear. Brevdo & Merkine found out that for flows at infinity that are strongly sheared vertically and of one sign it is possible to obtain fully attached boundary layers which possess an inner region of flow reversal. No numerical difficulties were encountered while integrating the nonlinear equations across $O(1)$ streamwise distances through these flow-reversal regions. This surprising result pivots on the linear dynamics of slightly viscous rotating systems, which generally remains uniformly valid in the presence of small nonlinear effects. Thus, if the linear problem supports flow-reversal regions, this property cannot be fundamentally altered when small nonlinearity is added, since the dynamics is that of regular perturbation. Brevdo & Merkine showed that when the degree of nonlinearity exceeds a certain non-zero threshold value the vertical boundary layer detaches from the wall, i.e. true separation occurs. However, this result is not directly related to the occurrence of flow-reversal regions within fully attached boundary layers.

It is of considerable interest to determine whether flow-reversal regions can exist in rotating systems that are continuously stratified. To this end it suffices to consider the linear dynamics which is investigated here. Barcilon & Pedlosky (1967*a*,*b*, hereinafter referred to as A and B respectively) investigated thoroughly the linear dynamics of contained rotating stratified fluids and showed how the vertical velocity and consequently the resulting dynamics depend crucially on the relation between the Ekman number E and the stratification parameter σS. The exact definition of these parameters will be given shortly. σS, however, is the product of the Prandtl number and the inverse rotational Froude number. Their findings show that when $\sigma S \ll E^{\frac{2}{3}}$ the fluid behaves as if it were essentially homogeneous, while for $\sigma S \gg E^{\frac{1}{2}}$ it is dominated by stratification. In the intermediate region $E^{\frac{2}{3}} \ll \sigma S \ll E^{\frac{1}{2}}$ the dynamics is of hybrid nature, exhibiting features of both homogeneous and stratified fluids. The strongly stratified region was investigated in A and the intermediate region in B. In the intermediate region standard Ekman layers are present along the horizontal boundaries, and the vertical boundary layer splits into three layers which are respectively the innermost buoyancy layer of thickness $(\sigma S)^{-\frac{1}{4}} E^{\frac{1}{2}}$, the intermediate hydrostatic baroclinic layer of thickness $(\sigma S)^{\frac{1}{2}}$ and the outer homogeneous layer of thickness $E^{\frac{1}{4}}$. In the strongly stratified limit the Ekman layers no longer control the interior dynamics, and in fact they are frequently absent. Along the vertical walls only the buoyancy layer remains, whose thickness is $E^{\frac{1}{2}}$.

The present investigation, although guided heavily by A and B, differs from these two important works in one major point, namely that exterior flows are considered. This leaves us with the additional degree of freedom of choosing the flow at infinity and hence exerting external control on the structure of the flow next to the vertical wall, which in our case is a right-circular cylinder. Two parameter regimes are considered: $\sigma S = O(1)$ and $\sigma S = O(E^{\frac{1}{2}})$. In the second regime the vertical velocity induced by the stratification is comparable to that induced by the Ekman suction, and the hydrostatic baroclinic vertical layer merges with the $E^{\frac{1}{4}}$ homogeneous layer. The thickness of the buoyancy layer becomes $E^{\frac{3}{8}}$. In other words, the vertical boundary layer consists now of only two sublayers. The triple structure obtained in B is a consequence of the weaker stratification considered there, since σS was restricted to the range $E^{\frac{2}{3}} \ll \sigma S \ll E^{\frac{1}{2}}$.

2. Formulation

Consider an incompressible viscous heat-conducting fluid confined between two horizontal planes a distance D apart. A horizontally uniform vertically sheared flow with characteristic velocity V is forced past a vertical circular cylinder of radius $r_0 D$ which extends throughout the depth of the fluid. The whole system rotates with a constant angular velocity Ω, its axis of rotation perpendicular to the horizontal planes. The appropriate linearized non-dimensional equations (V and D are the reference scales) for steady motions as given in B are

$$\hat{\boldsymbol{k}} \times \boldsymbol{u} = -\nabla p + T\hat{\boldsymbol{k}} + \tfrac{1}{2}E\nabla^2 \boldsymbol{u}, \tag{2.1}$$

$$\nabla . \boldsymbol{u} = 0, \tag{2.2}$$

$$\sigma S w = \tfrac{1}{2}E\nabla^2 T. \tag{2.3}$$

The vertical component of the velocity vector $\boldsymbol{u}$ is $w = \hat{\boldsymbol{k}} \cdot \boldsymbol{u}$. The dynamic pressure and temperature are denoted by p and T respectively. The ratio of the kinematic viscosity ν to the heat conductivity k is defined by the Prandtl number σ. $E = \nu/\Omega D^2$ is the Ekman number and $S = \alpha \Delta T g/4\Omega^2 D$ is the rotational stratification parameter. g is the acceleration of free fall and α is the coefficient of thermal expansion. $\Delta T \geqslant 0$ is the basic temperature difference of the equilibrium state, and it is assumed that $\alpha \Delta T \ll 1$. Our analysis assumes that $E \ll 1$, and, as stated in §1, two cases are of interest: $\sigma S = O(E^{\frac{1}{2}})$ and $\sigma S = O(1)$. Nonlinear effects are constrained to be small by requiring that $\epsilon = o(E^{\frac{1}{2}})$ in the former case and $\epsilon = o(E)$ in the latter case, where $\epsilon = V/2\Omega D$ is the Rossby number based on the characteristic velocity at large distances from the cylinder. In terms of the Reynolds number Re, the linear analysis is restricted to $Re = o(1/E^{\frac{1}{2}})$ for $\sigma S = O(E^{\frac{1}{2}})$ and $Re = o(1)$ for $\sigma S = O(1)$. The latter case is not directly applicable to geophysical applications since the Reynolds number is too small. However, such flows cannot be characterized as the extension of creeping Stokes flows to rotating stratified systems since diffusive effects are important only in boundary layers, and the interior flow, although controlled by diffusion, is inviscid to $O(E)$.

Equations (2.1)–(2.3) are supplemented by the boundary conditions

$$\boldsymbol{u} = 0, \quad \hat{\boldsymbol{n}} \cdot \nabla T = 0 \quad \text{on } z = 0, 1 \text{ and } r = r_0, \tag{2.4}$$

and

$$p = -[a + b(z - \tfrac{1}{2})]\, y \quad \text{as } r \to \infty, \tag{2.5}$$

where r is the polar radial coordinate. $z = 0, 1$ and $r = r_0$ denote the lower horizontal boundary, the upper horizontal boundary and the radius of the cylinder respectively. Equation (2.5) implies that at large distances from the cylinder the interior motion is in exact geostrophic balance and it is directed in the x-direction (unit vector $\hat{\boldsymbol{i}}$). The condition of no heat flux through the rigid boundaries simplifies the analysis (B) and allows direct comparison with laboratory conditions, which utilize salinity rather than temperature as the stratification agent.

3. The case of moderate stratification, $\sigma S = O(E^{\frac{1}{2}})$

In the interior, i.e. away from the horizontal Ekman layers at $z = 0, 1$ and the vertical layers at $r = r_0$, the following expansion of the field variables can be used:

$$\boldsymbol{q} = \boldsymbol{q}^0 + E^{\frac{1}{2}}\boldsymbol{q}^1 + \ldots, \quad w = E^{\frac{1}{2}}w^0 + \ldots, \quad p = p^0 + E^{\frac{1}{2}}p^1 + \ldots, \quad T = T^0 + E^{\frac{1}{2}}T^1 + \ldots,$$

where $\boldsymbol{q}$ denotes the horizontal part of the velocity vector. Since the interior flow is in geostrophic balance to $O(E)$, it follows from (2.1)–(2.2) that

$$\left.\begin{aligned} \boldsymbol{q}^0 &= \hat{\boldsymbol{k}}\times\nabla p^0, \quad T^0 = p^0_z, \\ \boldsymbol{q}^1 &= \hat{\boldsymbol{k}}\times\nabla p^1, \quad T^1 = p^1_z, \\ w^0_z &= 0, \quad \frac{2\sigma S}{E^{\frac{1}{2}}} w^0 = \nabla^2 T^0; \end{aligned}\right\} \tag{3.1}$$

implying that the leading-order motion is governed by the equation

$$\nabla^2 p^0_{zz} = 0. \tag{3.2}$$

It was shown in B that even for σS as large as $O(1)$ the dynamics of the Ekman layers is not affected by stratification. Consequently the Ekman-suction condition $w = \frac{1}{2}(-1)^z E^{\frac{1}{2}}\zeta$, $z = 0, 1$, (ζ is the vertical component of the relative vorticity) for homogeneous fluids can be used. When the vertical velocity at the edge of the Ekman layer is expressed in terms of the Laplacian of the temperature, we find that

$$\left.\begin{aligned} \frac{E^{\frac{1}{2}}}{\sigma S}\nabla^2 p^0_z &= \nabla_1^2 p^0 \quad \text{on } z = 0, \\ \frac{E^{\frac{1}{2}}}{\sigma S}\nabla^2 p^0_z &= -\nabla_1^2 p^0 \quad \text{on } z = 1, \end{aligned}\right\} \tag{3.3}$$

where ∇_1^2 is the horizontal part of the Laplacian. From (2.3) it follows that the correction to the temperature field induced by the Ekman layer is $O(E)$. This, in conjunction with the no-heat-flux wall condition, implies that

$$p^0_{zz} = 0 \quad \text{on } z = 0, 1. \tag{3.4}$$

Equation (3.2) can be integrated twice with respect to z to yield

$$\nabla^2 p^0 = F(x, y) + zG(x, y).$$

When this expression is substituted into (3.3) and use is made of (3.4) we find that the arbitrary functions of integration F and G must vanish, implying that the equation for the leading-order interior motion is

$$\nabla^2 p^0 = 0. \tag{3.5}$$

The circulation included in the general solution of (3.5) is removed by applying the argument of Walker & Stewartson (1972). An $O(1)$ steady circulation would lead to an axisymmetric unidirectional radial mass flux of $O(E^{\frac{1}{2}})$ in the Ekman layers. But such a radial mass flux can only be maintained by a distribution of sources or sinks along the cylinder, and this is not the case at hand. It follows that the solution for the leading-order interior motion is

$$p^0 = -[a + b(z - \tfrac{1}{2})]\left(\frac{r^2 - r_0^2}{r}\right)\sin\theta, \tag{3.6}$$

where θ is the polar angle measured from the positive x-direction. It follows from (3.6) that the leading-order interior motion is irrotational on each horizontal plane. The solution (3.6) does not satisfy the conditions of no slip and no heat flux at $r = r_0$, and a boundary-layer correction is required. This boundary layer consists of two sublayers, the thickest of which is of $O(E^{\frac{1}{4}})$. The $E^{\frac{1}{4}}$ layer is necessary for imposing the wall conditions on the leading-order horizontal motion and temperature field. The

inner $E^{\frac{3}{8}}$ layer is required for applying the no-slip condition to the leading-order vertical velocity.

The scaling of the variables in the $E^{\frac{1}{4}}$ layer is similar to the barotropic scaling of Walker & Stewartson (1972), augmented by a temperature field which enters the leading-order balance. Consequently we write

$$\left.\begin{aligned} &\mu = (r-r_0)/E^{\frac{1}{4}}, \\ &v = \hat{v}, \quad u = E^{\frac{1}{4}}\tilde{u}, \quad w = E^{\frac{1}{4}}\tilde{w}, \\ &p = E^{\frac{1}{4}}\tilde{p}, \quad T = E^{\frac{1}{4}}\tilde{T}, \end{aligned}\right\} \tag{3.7}$$

where all the tilde variables are $O(1)$ as $E \to 0$. u and v are the radial and azimuthal velocity components respectively. Equations (3.7) are now substituted into (2.1)–(2.3), and it follows that the motion is in geostrophic and hydrostatic balance to $O(E^{\frac{1}{4}})$, i.e.

$$\tilde{u} = -\frac{1}{r_0}\tilde{p}_\theta, \quad \tilde{v} = \tilde{p}_\mu, \quad \tilde{T} = \tilde{p}_z. \tag{3.8}$$

The equations for the vertical component of vorticity and the temperature field become

$$\tilde{w}_z + \tfrac{1}{2}\tilde{v}_{\mu\mu\mu} = 0, \quad \tilde{w} = \frac{E^{\frac{1}{2}}}{2\sigma S}\tilde{T}_{\mu\mu}, \tag{3.9}$$

from which the following equation for the azimuthal velocity emerges:

$$[\beta\tilde{v}_{\mu\mu} + \tilde{v}_{zz}]_\mu = 0, \quad \beta = \frac{\sigma S}{E^{\frac{1}{2}}}. \tag{3.10}$$

The Ekman-suction condition still applies, and we find that

$$\left.\begin{aligned} &\beta\tilde{v}_\mu - \tilde{v}_{z\mu} = 0 \quad \text{on } z = 0, \\ &\beta\tilde{v}_\mu + \tilde{v}_{z\mu} = 0 \quad \text{on } z = 1. \end{aligned}\right\} \tag{3.11}$$

The azimuthal velocity is subjected also to the wall condition

$$\tilde{v} = 0 \quad \text{on } \mu = 0 \tag{3.12}$$

and the matching condition

$$\tilde{v} = -2[a + b(z-\tfrac{1}{2})]\sin\theta \quad \text{as } \mu \to \infty. \tag{3.13}$$

Thus the solution for $\tilde{v}$ is uniquely specified by (3.10)–(3.13). We note that (3.12) and the thermal-wind relation $\tilde{v}_z = \tilde{T}_\mu$, which follows from (3.8), guarantee that to leading order the no-heat-flux condition is satisfied at the vertical wall.

The solution for $\tilde{v}$ can be written as

$$\tilde{v} = F(\theta, z) + \sum_{n=1}^{\infty} C_n(\theta) f_n(z)\, \mathrm{e}^{-\lambda_n \mu}, \quad \lambda_n > 0,$$

where the f_n are the solutions of the eigenvalue problem

$$\left.\begin{aligned} &f_{nzz} + \beta\lambda_n^2 f_n = 0, \\ &\beta f_n - f_{nz} = 0 \quad \text{on } z = 0, \\ &\beta f_n + f_{nz} = 0 \quad \text{on } z = 1. \end{aligned}\right\} \tag{3.14}$$

The non-trivial solutions of (3.14) are given by

$$f_n = \sin(\beta^{\frac{1}{2}}\lambda_n z + \phi_n), \tag{3.15}$$

where

$$\phi_n = \sin^{-1}\frac{\lambda_n}{(\lambda_n^2+\beta)^{\frac{1}{2}}}. \tag{3.16}$$

The eigenvalues λ_n are the solutions of the transcendental equation

$$\tan(\beta^{\frac{1}{2}}\lambda_n) = \frac{2\beta^{\frac{1}{2}}\lambda_n}{\lambda_n^2-\beta}. \tag{3.17}$$

The matching condition (3.13) determines $F(\theta, z)$, and the wall condition determines the C_n. The final expression for $\tilde{v}$ is

$$\left.\begin{aligned} \tilde{v} &= -2\left\{a+b(z-\tfrac{1}{2})-2\sum_{n=1}^{\infty} a_n\, \mathrm{e}^{-\lambda_n\mu}\sin(\chi_n z+\phi_n)\right\}\sin\theta \\ a_n &= \\ &\frac{2(a-\frac{1}{2}b)\,\chi_n\sin(\phi_n+\frac{1}{2}\chi_n)\sin(\frac{1}{2}\chi_n)+2b\cos(\phi_n+\frac{1}{2}\chi_n)\sin(\frac{1}{2}\chi_n)-b\chi_n\cos(\phi_n+\chi_n)}{\chi_n[\chi_n-\cos(\chi_n+2\phi_n)\sin(\chi_n)]}, \\ \chi_n &= \beta^{\frac{1}{2}}\lambda_n. \end{aligned}\right\} \tag{3.18}$$

The structure of the solution depends crucially on the distribution of the eigenvalues λ_n. For any given stratification, i.e. when β is fixed, $\lambda_n \sim (n-1)\pi/\beta^{\frac{1}{2}}$ as $n\to\infty$. The width of the layer, which is determined by the lowest eigenvalue, decreases with β. For example, $\lambda_1 \approx 1.403$, 1.307 and 0.831 for $\beta = 0.1$, 1 and 10 respectively. When $\beta\to 0$, $\lambda_1 \sim 2^{\frac{1}{2}}$ and $\lambda_n \sim (n-1)\pi/\beta^{\frac{1}{2}}$, $n > 1$. Thus, when the stratification is small but not zero, i.e. $\beta \ll 1$, the lowest eigenfunction is almost depth-independent (see (3.15) and (3.16)) and the width of layer equals that of the barotropic $E^{\frac{1}{4}}$ layer. However, since the interior flow is vertically sheared, the conditions of no slip and no heat flux cannot be satisfied by the barotropic part of the motion and all of the baroclinic eigenfunctions must be included their dynamics is felt within an inner region $O(\beta^{\frac{1}{2}}/\pi)$. As β increases, the baroclinic effects penetrate inward from the wall and the vertical boundary layer widens appreciably. $\lambda_1 \sim \pi/\beta^{\frac{1}{2}}$ as $\beta\to\infty$, and, for any fixed n, $f_n \sim \sin(n\pi z)$ as $\beta\to\infty$. When $\sigma S = O(1)$ the vertical boundary layer fills the entire interior. These conclusions, which are of a general nature, can also be extracted from A and B. Nevertheless, the present study differs in one major aspect. Barcilon & Pedlosky treated contained flows with interior vertical shear which is always proportional to σS. We consider exterior flows with vertical shear which is determined by the flow at infinity independently of σS for non-zero σS. Consequently we can have an $O(1)$ vertical shear in the interior although $\sigma S = O(E^{\frac{1}{2}})$.

We proceed now to present particular solutions which reveal some peculiar dynamical effects. We consider first the case of interior flow that is depth-independent, i.e., $a = 1$, $b = 0$. For non-zero stratification the structure of the vertical boundary layer must be depth-dependent since none of the eigenfunctions is pure barotropic. However, as β decreases the lowest eigenfunction approaches its barotropic structure and the importance of the higher eigenfunctions weakens; their effect is felt closer to the wall. In this limiting case the eigenfunctions approach the structure given in A for $\sigma S \ll E^{\frac{1}{2}}$. This behaviour is depicted in figure 1, which shows the radial structure of the azimuthal velocity $\tilde{v}$ at $z = 0$ and 0.5 for the two cases $\beta = 0.1$ and 10. For this interior-velocity profile the horizontal motion is symmetric about $z = 0.5$. We observe that in the case of $\beta = 0.1$ the structure is almost barotropic. However, when

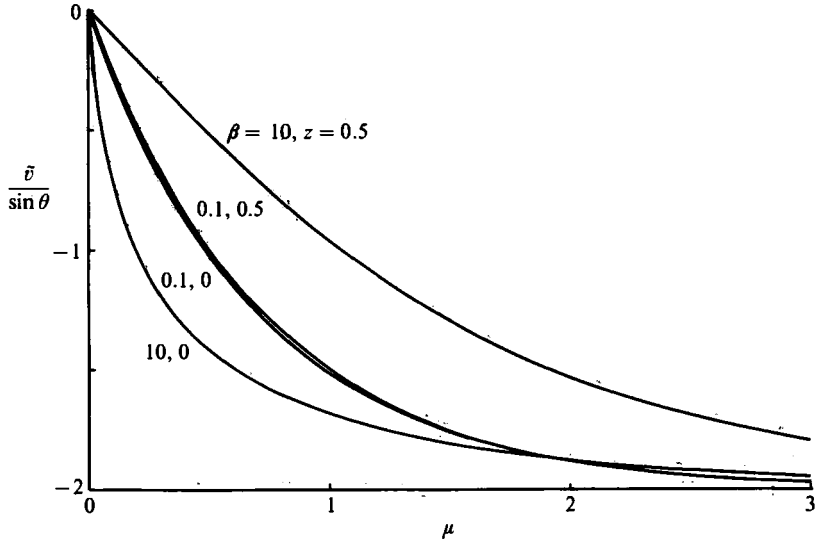

FIGURE 1. The radial structure (the $\sin\theta$ term extracted) of the boundary-layer azimuthal velocity corresponding to an oncoming flow possessing no vertical shear, i.e. $a = 1, b = 0$. $\tilde{v}$ is negative when it is in the same overall direction as the oncoming flow, which is directed along the positive x-direction. $\beta = \sigma S/E^{\frac{1}{2}}$.

$\beta = 10$ the azimuthal velocity exhibits strong vertical variation and weaker radial decay, in agreement with the earlier discussion. We observe also that the velocity gradient at the wall is greater at $z = 0$ than at $z = 0.5$. For fixed β and large n, $\chi_n \sim (n-1)\pi + 2\beta/(n-1)\pi$, $\phi_n \sim \frac{1}{2}\pi - \beta/(n-1)\pi$ and consequently $a_n = O(1/n^2)$. It follows that the corresponding coefficients in the series for the wall shear stress are $O(1/n)$. Inspection shows that the series for the wall shear stress at $z = 0$, 1 diverges like the harmonic series $\Sigma(1/n)$, which implies logarithmic singularity in the wall shear stress at $z = 0, 1$ for the interior velocity profiles that are height-independent or depend linearly on z. The wall shear stress corresponding to figure 1 is depicted in figure 2(*a*). It is weaker for stronger stratification, since the boundary layer widens, and it becomes more uniform as the stratification weakens.

When the interior horizontal motion is vertically sheared the baroclinic eigenfunctions are important even when the stratification is weak. Figure 3 depicts the azimuthal velocity profile in the boundary layer for an interior velocity profile that vanishes at $z = 0$ and possesses a unit vertical shear at infinity, i.e. $a = \frac{1}{2}, b = 1$. For this profile the horizontal motion is no longer symmetric about $z = 0.5$. Similarly to figure 1, we observe the widening of the vertical layer with β, but the most striking feature is the appearance of an intense reversed-flow region in the immediate vicinity of the wall in the lower part of the cylinder. When β decreases, the intensity of the reverse flow region increases, with a maximum that is closer to the wall.† The vertical distribution of the wall shear stress depicted in figure 2(*b*) reveals that when the stratification is large, in the sense that $\beta \gg 1$, the backflow region is confined to the vicinity of the lower horizontal surface. However, it penetrates into higher vertical levels as β decreases.

† This trend cannot be continued to the limit $\beta = 0$ since the analysis is based on the premise that stratification always exists. Otherwise, the Taylor–Proudman theorem would not allow vertical shear at infinity. Thus when $\beta \to 0$ the shear at infinity must be relaxed to $O(\beta)$ and an analysis similar to A that assumes triple structure for the boundary layer must be performed.

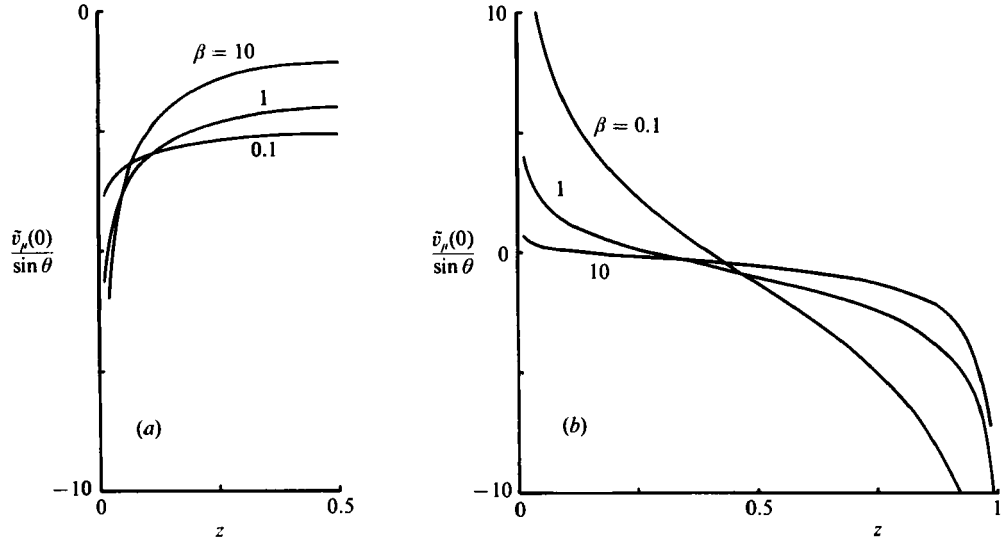

FIGURE 2. The vertical distribution of the wall shear stress (the $\sin\theta$ term extracted). Positive shear indicates backflow next to the cylinder. (*a*) The oncoming flow possesses no vertical shear, i.e. $a = 1$, $b = 0$. (*b*) The oncoming flow vanishes on $z = 0$ and possess a unit vertical shear, i.e. $a = \frac{1}{2}$, $b = 1$. $\beta = \sigma S/E^{\frac{1}{2}}$.

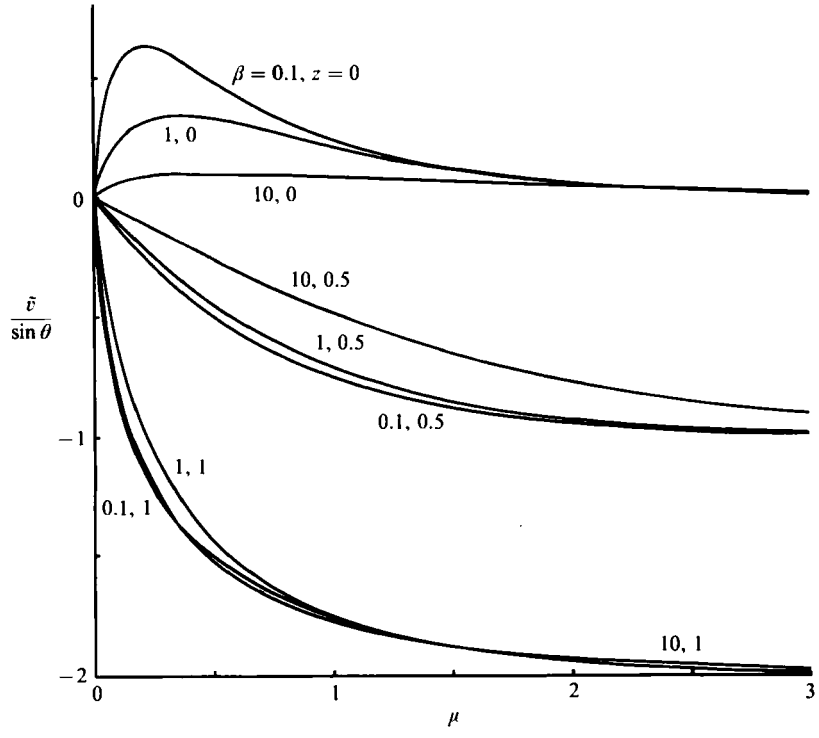

FIGURE 3. The radial structure (the $\sin\theta$ term extracted) of the boundary-layer azimuthal velocity corresponding to an oncoming flow that vanishes on $z = 0$ and possesses unit vertical shear, i.e. $a = \frac{1}{2}$, $b = 1$. Positive $\tilde{v}$ corresponds to flow reversal. $\beta = \sigma S/E^{\frac{1}{2}}$.

The existence of a region next to the wall possessing azimuthal velocity in opposite direction to its asymptotic value just outside the boundary layer is strange, since unlike the Ekman layers the vertical layers are controlled by the interior flow rather than controlling it. Physical understanding of the flow-reversal phenomenon and, as a matter of fact, of the entire vertical structure of the $E^{\frac{1}{4}}$ layer is not difficult, however. The interior flow (3.6) impresses at the wall $r = r_0$ a temperature gradient given by $-2b\sin\theta$. For $b > 0$, as in our example, and (say) for $0 < \theta < \pi$ this gradient is negative. The wall no-heat-flux condition requires that the boundary layer responds by generating a wall temperature gradient of equal magnitude but of opposite sign. The Ekman-suction condition (3.11) for the boundary-layer correction, referring now only to the exponentially decaying part of the boundary-layer solution, can be written, using the thermal-wind relation $\tilde{v}_z = \tilde{T}_\mu$, as $\beta\tilde{v} = \pm\tilde{T}_\mu$, where + and − refer to $z = 0$ and 1 respectively. We see now that the generation of a positive temperature gradient by the boundary-layer correction must be accompanied by an azimuthal-velocity correction that is positive at $z = 0$ and negative at $z = 1$. Since an $O(1)$ temperature gradient is induced by the boundary-layer correction the Ekman-suction condition implies that the azimuthal velocity correction intensifies inversely proportionally to β. In the example of figure 3 the interior flow vanishes at $z = 0$, leaving the vicinity of this region to be dominated by the counterflow effect. The degree of vertical penetration of the flow-reversal regions can be best appreciated from the vertical distribution of the wall shear stress depicted in figure 2(*b*). When stratification decreases, the baroclinic part of the $E^{\frac{1}{4}}$ layer narrows, the shear increases, the azimuthal velocity correction increases and the vertical penetration increases. Alternatively, strong stratification inhibits the vertical velocity, rendering the Ekman-suction condition less effective in controlling the dynamics.

Since the linear analysis is uniformly valid, it is expected that the existence of a counterflow region next to the wall should not be altered when small nonlinearity is added. Consequently it is important to demonstrate that our analysis is correct to leading order. The $E^{\frac{1}{4}}$ layer is necessary for imposing the no-slip and no-heat-flux wall conditions on the leading-order horizontal motion and temperature field. Thus it is still necessary to impose the no-slip wall condition on the vertical velocity. To this end it is necessary to have an inner boundary layer, the buoyancy layer of B, which in our case is $O(E^{\frac{2}{5}})$ wide with the following scaling for the field variables: $u = O(E^{\frac{4}{5}})$, $v = O(E^{\frac{4}{5}})$, $w = O(E^{\frac{1}{5}})$, $p = O(E^{\frac{2}{5}})$ and $T = O(E^{\frac{1}{5}})$. This implies that the wall shear stress induced by the buoyancy layer is $O(1)$ and hence negligibly small in an asymptotic sense compared with the $O(E^{-\frac{1}{4}})$ wall shear stress induced by the $E^{\frac{1}{4}}$ layer. In view of the dynamic insignificance of the buoyancy layer to the wall shear stress and to the phenomenon of flow reversal, we shall not pursue it any further. We proceed now to discuss the case of strong stratification.

4. The case of strong stratification, $\sigma S = O(1)$

It is shown in A that when $\sigma S = O(1)$ the interior vertical velocity is $O(E)$. Following the analysis presented there, we obtain, using our notation, the geostrophic–hydrostatic balance

$$\boldsymbol{q}^0 = \hat{\boldsymbol{k}} \times \nabla p^0, \quad T^0 = p^0_z \tag{4.1}$$

for the leading-order interior motion, which is governed by

$$\nabla^2\left(\nabla_1^2 + \frac{1}{\sigma S}\frac{\partial^2}{\partial z^2}\right)p^0 = 0, \tag{4.2}$$

subject to the boundary condition

$$\nabla_1^2 p^0 = 0 \qquad \text{on } z = 0, 1, \tag{4.3}$$

$$p^0_{zz} = 0 \qquad \text{on } z = 0, 1, \tag{4.4}$$

$$p^0_r = p^0_\theta = 0 \quad \text{on } r = r_0. \tag{4.5}$$

(See top of page 7 of A as well as (3.13′), (5.11) and (5.12) of that paper with the forcing terms equal to zero and $a_T = a_B = 0$.) By virtue of the thermal-wind relation the no-heat-flux wall condition is also satisfied to lowest order. Equations (4.2)–(4.5) when supplemented by the pressure distribution at infinity, namely (2.5), are sufficient for determining the lowest-order interior motion. It is convenient to introduce the pressure deviation

$$\varphi = p^0 + [a + b(z - \tfrac{1}{2})]\left(\frac{r^2 - r_0^2}{r}\right)\sin\theta, \tag{4.6}$$

in terms of which the problem becomes

$$\nabla^2 Q = 0, \quad Q = \left(\nabla_1^2 + \frac{1}{\sigma S}\frac{\partial^2}{\partial z^2}\right)\varphi, \tag{4.7}$$

$$\varphi = Q = 0 \quad \text{on } z = 0, 1 \text{ and as } r \to \infty, \tag{4.8}$$

$$\varphi = 0 \quad \text{on } r = r_0, \tag{4.9}$$

$$\varphi_r = 2r_0[a + b(z - \tfrac{1}{2})]\sin\theta \quad \text{on } r = r_0. \tag{4.10}$$

The desired solution for Q is

$$Q = \sin\theta \sum_{n=1}^{\infty} A_n \sin(n\pi z)\, K_1(r_n), \quad r_n = n\pi r, \tag{4.11}$$

where A_n are arbitrary constants. The solution for φ satisfying all but the wall conditions† is

$$\varphi = \sin\theta \sum_{n=1}^{\infty} \left[A_n \frac{\sigma S K_1(r_n)}{n^2\pi^2(\sigma S - 1)} + B_n K_1\left(\frac{r_n}{(\sigma S)^{\frac{1}{2}}}\right)\right] \sin(n\pi z), \tag{4.12}$$

where B_n are arbitrary constants. The constants A_n and B_n are determined by imposing on φ the wall conditions (4.9) and (4.10), and we obtain the final result for p^0:

$$\begin{aligned} p = &-[a + b(z - \tfrac{1}{2})]\left(\frac{r^2 - r_0^2}{r}\right)\sin\theta \\ &+ (\sigma S)^{\frac{1}{2}}\sin\theta \sum_{n=1}^{\infty} \left(\frac{2}{n\pi}\right)^2 [(a - \tfrac{1}{2}b)(1 + (-1)^{n+1}) + b(-1)^{n+1}] \\ &\times \frac{K_1(r_{0n})\, K_1(r_n/(\sigma S)^{\frac{1}{2}}) - K_1(r_{0n}/(\sigma S)^{\frac{1}{2}})\, K_1(r_n)}{(\sigma S)^{\frac{1}{2}} K_1(r_{0n}/(\sigma S)^{\frac{1}{2}})\, K_0(r_{0n}) - K_0(r_{0n}/(\sigma S)^{\frac{1}{2}})\, K_1(r_{0n})} \sin(n\pi z), \end{aligned} \tag{4.13}$$

where $r_{0n} = n\pi r_0$.

The first part of the solution‡ (4.13) is a potential flow with harmonic horizontal motion. It is independent of the stratification parameter and it satisfies the equation

† It is shown in A that a vertical boundary layer of width $E^{\frac{1}{4}}$ without substructure can exist when $\sigma S = O(1)$. However, it is eliminated in the case of the no-heat-flux wall condition.

‡ Equation (4.13) is not singular at $\sigma S = 1$. The appropriate expression is evaluated by applying the limit $\sigma S \to 1$ to (4.13).

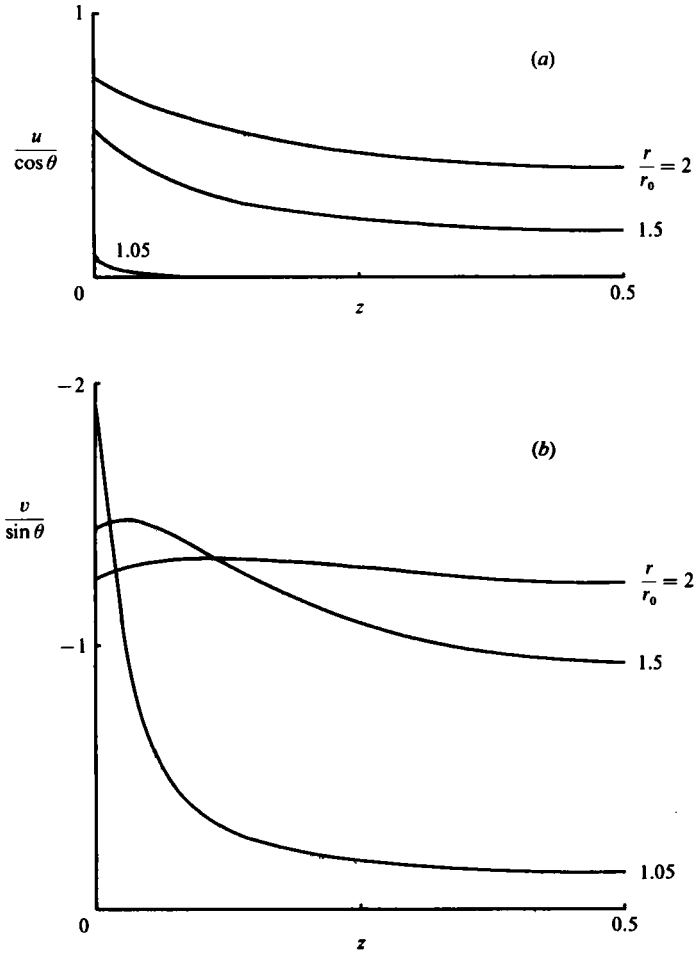

FIGURE 4. The vertical structure of the horizontal velocity components at different radial locations for $(\sigma S)^{\frac{1}{2}} = 10$ and $r_0 = \frac{1}{2}$. The oncoming flow possesses no vertical shear, i.e. $a = 1$, $b = 0$. (*a*) The radial velocity (the $\cos\theta$ term extracted). (*b*) The azimuthal velocity (the $\sin\theta$ term extracted).

and the boundary conditions, leaving out the no-slip condition for the azimuthal velocity and the associated no-heat flux constraint. These are satisfied by including the second part of the solution, which is stratification-dependent and confined to the vicinity of the cylinder. From the asymptotic properties of modified Bessel functions it follows that the degree of penetration of the stratification effects from the vertical wall into the interior depends, for a given σ, on the ratio of the cylinder radius to the radius of deformation $(\alpha \Delta T g D/4\Omega^2)^{\frac{1}{2}}$ and is equal to the larger of the two.

Figures 4 and 5 illustrate two particular solutions corresponding to $r_0 = 0.5$ and $(\sigma S)^{\frac{1}{2}} = 10$. Thus the fluid is heavily stratified and the diameter of the cylinder is equal to the depth of the fluid. Similar qualitative results are obtained for other values of the parameters. We consider first the case of $a = 1$ and $b = 0$, corresponding to a velocity profile possessing no vertical shear at infinity. Figure 4 depicts the vertical structure of the azimuthal and radial velocity components at several radial locations. The profiles are symmetric about $z = \frac{1}{2}$. No flow reversal occurs, and this is consistent with the results obtained in §3 for the same velocity profile at infinity. The striking feature, however, is that the azimuthal velocity develops strong vertical shear in the

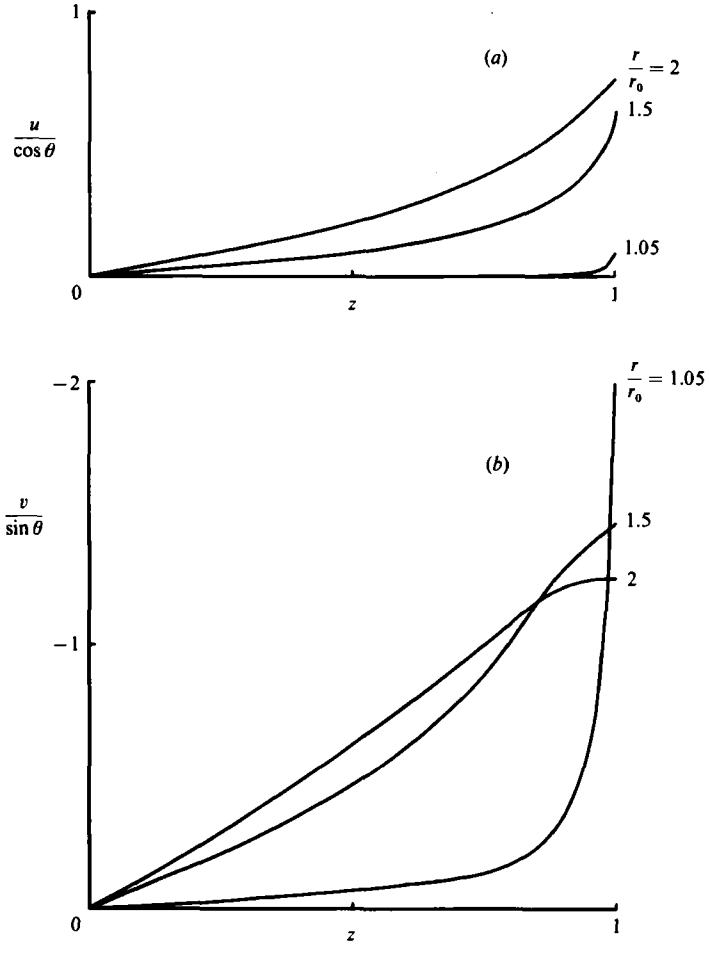

FIGURE 5. The same as in figure 4, but for an oncoming flow that vanishes on $z = 0$ and possesses a unit vertical shear, i.e. $a = \frac{1}{2}$, $b = 1$.

vicinity of r_0 and $z = 0, 1$. Figure 5 depicts the same velocity profiles, but for $a = \frac{1}{2}$, $b = 1$, i.e. for a linear velocity profile at infinity that vanishes on $z = 0$ and possesses a unit vertical shear. The results are no longer symmetric about $z = \frac{1}{2}$. Contrary to the results of §3, no flow reversal is observed next to the cylinder in the vicinity of $z = 0$. Ekman suction, which in §3 is responsible for the existence of the reversed-flow region, is eliminated here on account of the strong stratification. Similarly to figure 4, the azimuthal velocity develops strong vertical shear in the vicinity of the cylinder. This shear is confined, however, to the vicinity of $z = 1$ only.

The strong shear of the azimuthal velocity in the corner region results from the failure of this velocity component to satisfy the no-slip condition there. The pressure distribution on $z = 0, 1$ is derived from the solution of the harmonic equation (4.3), and as such it can only satisfy the wall condition for the radial velocity component. Consequently a discontinuity in the interior azimuthal velocity develops at the corner for all velocity profiles that do not vanish at infinity on $z = 0, 1$. The dimensions of the corner region in the radial and vertical directions are $E^{\frac{1}{3}} \times E^{\frac{1}{3}}$, and the lowest-order interior pressure distribution obtained from the solution of (4.3) is valid outside an

$O(E^{\frac{1}{2}})$ lateral distance from the cylinder. (The lowest-order interior pressure distribution is valid all the way to the vertical wall for all $0 < z < 1$ independently of the conditions at infinity as shown in A.) If the velocity profile at infinity vanishes on the horizontal boundary surfaces the corresponding Ekman layers disappear and the lowest-order corner region is eliminated. For a linear velocity profile at infinity this is possible on one horizontal surface at the most. Consequently one corner region always exists.

The failure of the $O(1)$ interior velocity to satisfy the no-slip boundary condition at one point is significant dynamically only if the removal of the discontinuity introduces $O(1)$ effects that are not local. When that occurs the interior flow cannot be fully determined unless the detailed structure of the corner region is considered. In contained flows it is possible to bypass this difficult issue by applying global conservation principles to the integrated mass flux (Greenspan 1968). Since the solution (4.13) is completely determined, it is not clear what additional information could emerge from such a procedure if it were possible to apply it usefully to our external-flow problem. The solution (4.13) may not be valid globally if the lowest-order vertical boundary layer, whose width is $O(E^{\frac{1}{3}})$, must not vanish and hence can absorb an $O(E^{\frac{1}{2}})$ vertical mass flux from the non-trivial Ekman layer. This implies, however, a corresponding $O(1)$ vertical velocity in this $E^{\frac{1}{3}}$ layer, which is not possible on account of the no-heat-flux wall condition.

A single equation can be derived for the pressure (Greenspan 1968), and in our notation it assumes the form

$$\nabla^2\left(\frac{E^2}{4\sigma S}\nabla^2\nabla^2\nabla^2 p+\nabla^2 p+\left(\frac{1}{\sigma S}-1\right)\frac{\partial^2 p}{\partial z^2}\right)=0.$$

In the corner region it reduces to

$$\delta^2\left(\frac{1}{4\sigma S}\delta^2\delta^2\delta^2 p+\delta^2 p+\left(\frac{1}{\sigma S}-1\right)\frac{\partial^2 p}{\partial \xi^2}\right)=0, \quad \delta^2=\frac{\partial^2}{\partial \mu^2}+\frac{\partial^2}{\partial \xi^2},$$

where $\mu = (r-r_0)/E^{\frac{1}{3}}$ and $\xi = z/E^{\frac{1}{3}}$ or $(1-z)/E^{\frac{1}{3}}$. No attempt is made here to solve this equation, but one of the requirements of its solution is that it must turn sideways the $O(E^{\frac{1}{3}})$ radial flux impinging on the corner region from the non-trivial Ekman layer. (This necessitates a strong tangential jet in the corner region.) If this cannot be achieved, then the assumptions relating to the uniformity of weak nonlinear effects or steadiness may have to be relinquished.† The rest of this section is devoted to interior velocity profiles that vanish on $z = 0, 1$, thus avoiding the difficult issue raised above.

The linear pressure distribution (2.5) provides an exact geostrophic balance to all orders of the interior flow at infinity. Such a balance does not always exist in geophysical or engineering flows, and it is of interest to understand how slight deviations from exact geotrophy of the interior pressure distribution at infinity affect the flow response. In other words, we are interested in velocity profiles at infinity that are not necessarily linear functions of the vertical coordinate. We have carried out such an analysis for the parameter range of §3. $O(E^{\frac{1}{3}})$ deviations were introduced, and the results revealed again the existence of flow-reversal regions. In the rest of this section we shall consider the effect of $O(E)$ deviations when $\sigma S = O(1)$.

† It would be useful if the theory presented here could be verified using the laboratory apparatus described by Boyer, Davies & Biolley (1984).

We now consider pressure distributions at infinity that are given by

$$\left.\begin{aligned} p^0 &= -U(z)\,y \quad \text{as } r\to\infty, \\ U(z) &= U_{zz}(z) = 0 \quad \text{on } z = 0, 1. \end{aligned}\right\} \tag{4.14}$$

The constraint on U is necessary for the interior solution to satisfy the Ekman-suction condition (4.3) by virtue of triviality, even for horizontal pressure distributions that are not harmonic in the vicinity of the horizontal boundaries. The constraint on U_{zz} is necessary for consistency with the no-heat-flux condition (4.4).

It is important to realize that an imposed $O(E)$ deviation from geostrophy requires the existence of externally imposed potential-vorticity sources, otherwise the steadiness assumption is violated. The cause of the existence of such sources can be solar radiation in the atmosphere and applied wind stress in the oceans. Thus if, for example, we augment the temperature equation (2.3) by a weak radiation source $\frac{1}{2}Eh(z)\,y$ and follow the expansion of A we find that the leading-order interior motion is governed by (4.2) augmented on the right-hand side by the source divergence $(-1/\sigma S)\,y\,\mathrm{d}h/\mathrm{d}z$. No sources are required for the pressure distribution (2.5), but for the more general profile (4.14) the appropriate extension of (4.2) is

$$\nabla^2\left(\nabla_1^2+\frac{1}{\sigma S}\frac{\partial^2}{\partial z^2}\right)p^0 = -\frac{r\sin\theta}{\sigma S}\frac{\mathrm{d}^4U}{\mathrm{d}z^4}. \tag{4.15}$$

We define φ by

$$\varphi = p^0 + U(z)\,y \tag{4.16}$$

and find that it is governed by the earlier equation and boundary conditions with $U(z)$ replacing $a+b(z-\frac{1}{2})$.

Let φ_n denote the solution corresponding to $U(z) = \sin(n\pi z)$; then

$$\begin{aligned} \varphi_n = \sin\theta\sin(n\pi z)\Bigg\{ & r_0\left[K_0(r_{0n})\,K_1\left(\frac{r_n}{(\sigma S)^{\frac{1}{2}}}\right)-K_0\left(\frac{r_{0n}}{(\sigma S)^{\frac{1}{2}}}\right)\frac{K_1(r_n)}{(\sigma S)^{\frac{1}{2}}}\right] \\ & +\frac{2}{n\pi}\left[K_1(r_{0n})\,K_1\left(\frac{r_n}{(\sigma S)^{\frac{1}{2}}}\right)-K_1\left(\frac{r_{0n}}{(\sigma S)^{\frac{1}{2}}}\right)K_1(r_n)\right]\Bigg\} \\ & \times\left\{K_0(r_{0n})\,K_1\left(\frac{r_{0n}}{(\sigma S)^{\frac{1}{2}}}\right)-K_0\left(\frac{r_{0n}}{(\sigma S)^{\frac{1}{2}}}\right)\frac{K_1(r_{0n})}{(\sigma S)^{\frac{1}{2}}}\right\}^{-1}. \end{aligned} \tag{4.17}$$

The wall shear stress is given by

$$\begin{aligned} \left.\frac{\partial v_n^0}{\partial r}\right|_{r=r_0} &= \left.\frac{\partial^2\varphi_n}{\partial r^2}\right|_{r=r_0} \\ &= \sin\theta\sin(n\pi z)\left\{\frac{n^2\pi^2 r_0}{\sigma S}\left[K_0(r_{0n})\,K_1\left(\frac{r_{0n}}{(\sigma S)^{\frac{1}{2}}}\right)\right.\right. \\ &\quad \left.-(\sigma S)^{\frac{1}{2}}K_0\left(\frac{r_{0n}}{(\sigma S)^{\frac{1}{2}}}\right)K_1(r_{0n})\right]+\frac{2n\pi}{\sigma S}(1-\sigma S)\,K_1\left(\frac{r_{0n}}{(\sigma S)^{\frac{1}{2}}}\right)K_1(r_{0n})\Bigg\} \\ &\quad \times\left\{K_0(r_{0n})\,K_1\left(\frac{r_{0n}}{(\sigma S)^{\frac{1}{2}}}\right)-K_0\left(\frac{r_{0n}}{(\sigma S)^{\frac{1}{2}}}\right)K_1(r_{0n})\right\}^{-1}, \end{aligned} \tag{4.18}$$

and for $\pi r_0 \gg \max(1, (\sigma S)^{\frac{1}{2}})$ we can use the asymptotic properties of modified Bessel functions for large arguments to find that

$$\left.\frac{\partial^2\varphi_n}{\partial r^2}\right|_{r=r_0} \sim -\left\{\frac{r_0 n^2\pi^2}{(\sigma S)^{\frac{1}{2}}}\sin(n\pi z)+\frac{15n\pi}{8(\sigma S)^{\frac{1}{2}}}(1+(\sigma S)^{\frac{1}{2}})\sin(n\pi z)\right\}\sin\theta. \tag{4.19}$$

It then follows that for a general velocity profile

$$U(z) = \sum_{n=1}^{\infty} C_n \sin(n\pi z), \tag{4.20}$$

which satisfies the constraints (4.14),

$$\left.\frac{\partial v^0}{\partial r}\right|_{r=r_0} \sim \frac{1}{(\sigma S)^{\frac{1}{2}}}\left[r_0 U_{zz} - \tfrac{15}{8}\pi(1+(\sigma S)^{\frac{1}{2}}) \sum_{n=1}^{\infty} nC_n \sin(n\pi z)\right]\sin\theta. \tag{4.21}$$

For sufficiently large r_0 (4.21) can be further approximated as

$$\left.\frac{\partial v^0}{\partial r}\right|_{r=r_0} \sim \frac{r_0}{(\sigma S)^{\frac{1}{2}}} U_{zz} \sin\theta, \tag{4.22}$$

thus revealing the striking result that, under the constraint leading to (4.22), velocity profiles satisfying $U(z) \geqslant 0$ develop reversed-circulation regions next to the cylinder in those vertical regions for which $U_{zz} > 0$. (Positive wall shear stress implies reverse circulation, since the flow at infinity is directed along the positive x-direction.) The lateral extent of the flow-reversal region can be comparable to the dimensions of the cylinder, as our particular examples will show. It should be emphasized that the existence of flow-reversal regions does not depend on the conditions leading to (4.21) or (4.22). These expressions serve to demonstrate the point visually. In more general cases the possible existence of the flow-reversal regions should be determined from the general solution.

A very simple example is provided by the velocity profile

$$U(z) = \sin^3(\pi z) = \tfrac{3}{4}\sin(\pi z) - \tfrac{1}{4}\sin(3\pi z), \tag{4.23}$$

for which (4.21) reduces to

$$\left.\frac{\partial v^0}{\partial r}\right|_{r=r_0} \sim -\frac{3\pi^2 r_0}{4(\sigma S)^{\frac{1}{2}}}\left\{\left[1+\frac{15}{8\pi r_0}(1+(\sigma S)^{\frac{1}{2}})\right]\sin(\pi z) + \left[3+\frac{15}{8\pi r_0}(1+(\sigma S)^{\frac{1}{2}})\right]\sin(3\pi z)\right\}\sin\theta. \tag{4.24}$$

Figure 6 depicts the wall shear stress as a function of z for a wide range of the parameters r_0 and $(\sigma S)^{\frac{1}{2}}$ not necessarily consistent with the above asymptotic estimates. The results are symmetric about $z = \frac{1}{2}$. All cases demonstrate the existence of two flow-reversal regions next to the cylinder and in the vicinity of the horizontal boundary surfaces at $z = 0$ and 1. The physical explanation of the features of figure 6 is similar to the one given in §3. The heat flux induced at the wall by $U(z)$ is parameter-independent and must be counteracted by the wall heat flux of the flow field induced by the cylinder. Consider the range $0 \leqslant z \leqslant \frac{1}{2}$, $0 \leqslant \theta \leqslant \pi$, for example. Next to $z = 0$, U is small and $U_z > 0$, and from the thermal-wind relation it follows that the induced temperature gradient must be negative. This temperature gradient decays away from the wall, implying positive T^0_{rr} and v^0_{rz} at the wall. This is the reason for the existence of the flow-reversal region. When the radius of deformation is less than the geometric scale, v^0_{rz} increases inversely proportional to $(\sigma S)^{\frac{1}{2}}$, as observed in figure 6 and indicated by (4.24). This explains the increase in the vertical extent of the flow-reversal region, which can occupy, in our example, more than half of the depth of the fluid. For the same reason the lateral extent of the flow-reversal region decreases with $(\sigma S)^{\frac{1}{2}}$.

The existence of counterflow next to the cylinder implies the existence of a domain

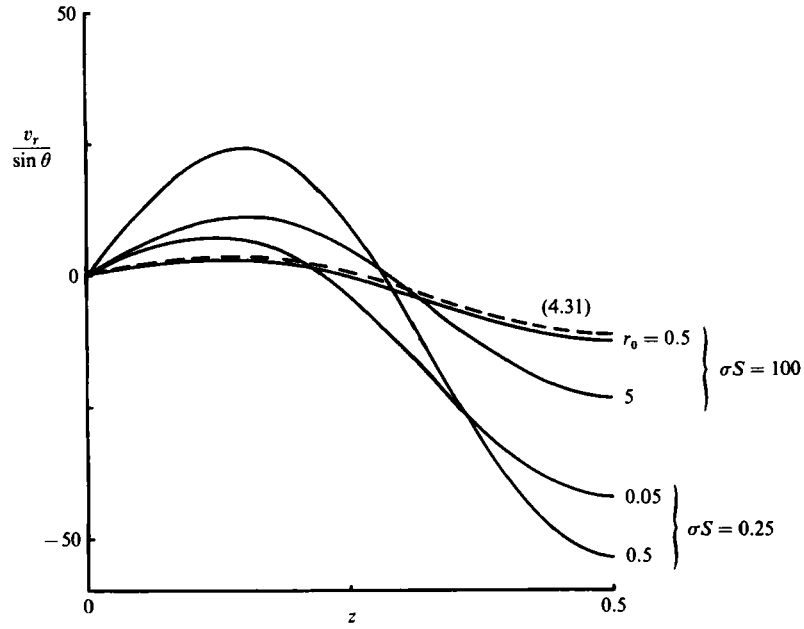

FIGURE 6. The vertical distribution of the wall shear stress (the $\sin\theta$ term extracted) for an oncoming flow given by $\sin^3(\pi z)$. The dashed line corresponds to the asymptotic estimate (4.31). Positive shear indicates backflow next to the cylinder.

containing the reversed-flow region that is not accessible to fluid particles coming from infinity. The boundary of this axisymmetric domain is determined by $p^0(z, r) = 0$. It follows from the arguments just presented that the lateral extent of this domain increases with stratification. At $z = 0.15$, corresponding approximately to the region of maximum positive shear according to figure 6, we find that, for $r_0 = 0.5$, $p^0 = 0$ extends to $2.7r_0$ and $1.76r_0$ for $(\sigma S)^{\frac{1}{2}} = 10$ and 0.5 respectively. For $r_0 = 0.05$ and $(\sigma S)^{\frac{1}{2}} = 0.5$ it extends to $4.4r_0$, and for $r_0 = 5$ and $(\sigma S)^{\frac{1}{2}} = 10$ it extends to $1.45r_0$. (Recall that r_0 is measured in units of depth.) Figure 6 indicates that increasing r_0 is qualitatively equivalent to decreasing $(\sigma S)^{\frac{1}{2}}$. This is so because of the combination $r_0/(\sigma S)^{\frac{1}{2}}$ that appears in the solution, and in particular in the asymptotic expression (4.19). Hence there is no need to interpret the results in terms of placing cylinders of various radii in a fluid with a given stratification. For the purpose of illustration, we show in figure 7 the radial dependence of the pressure, the azimuthal velocity v^0 and the radial velocity u^0 at $z = 0.15$ and 0.5 for $r_0 = 5$ and $(\sigma S)^{\frac{1}{2}} = 10$. In view of the above discussion, the features of this figure are self-explanatory.

5. Discussion

We have considered linear stratified rotating flows, but it is important to study how the existence of backflow regions next to the cylinder is modified by nonlinear effects. Since the linear solution is uniformly valid, we expect that small nonlinear effects will alter the results in a continuous way. Guided by the results of Brevdo & Merkine (1985) for the two-layer model, we speculate that, as nonlinearity increases, a favourable pressure gradient will develop next to the forward stagnation point, and it will push the backflow region downstream. At the same time an adverse pressure

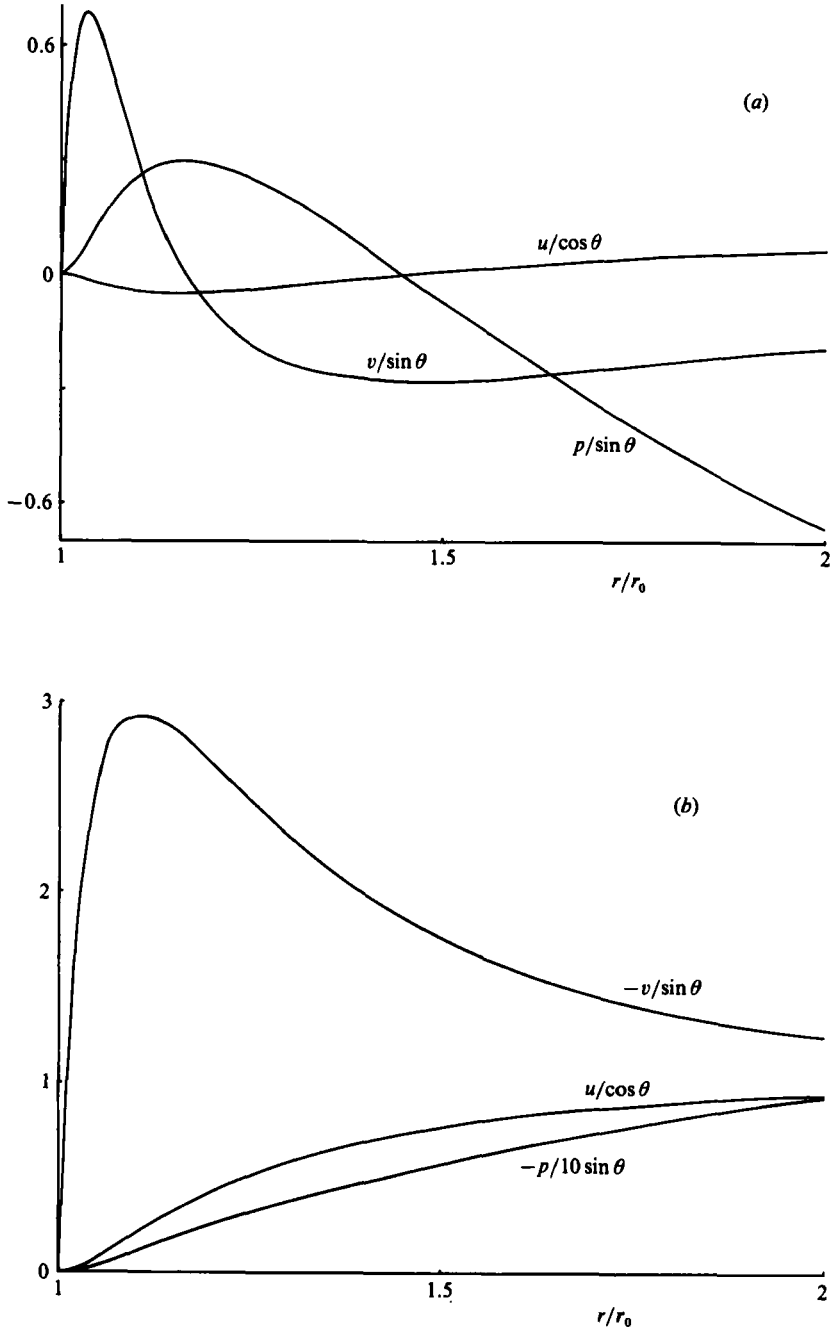

FIGURE 7. The radial structure of the pressure (the $\sin\theta$ term extracted), the azimuthal velocity (the $\sin\theta$ term extracted) and the radial velocity (the $\cos\theta$ term extracted) at $z = 0.15$ (*a*) and at $z = 0.5$ (*b*) for $r_0 = 5$, $(\sigma S)^{\frac{1}{3}} = 10$ and an oncoming flow given by $\sin^3(\pi z)$. Positive $\tilde{v}$ corresponds to backflow. At $z = 0.15$ the radial extent of the domain not accessible to fluid particles coming from infinity is given by $0 \leqslant r \lesssim 1.45 r_0$.

gradient will develop downstream, which, if strong enough, will cause separation at the rear stagnation point. The streamwise extent of the backflow region will diminish as nonlinearity increases, and finally it will be eliminated when the Rossby number becomes comparable to $E^{\frac{1}{2}}$ for $\sigma S = O(E^{\frac{1}{2}})$ or to E for $\sigma S = O(1)$.

The solution of the nonlinear problem requires a separate study. It is not difficult to show, however, that when $\sigma S = O(E^{\frac{1}{4}})$ and when $\epsilon = O(E^{\frac{1}{4}})$ the interior solution (3.6) is still valid whereas the nonlinear boundary layer is governed by

$$\frac{2\epsilon}{r_0 E^{\frac{1}{2}}} J\left(\tilde{p}, \tilde{p}_{\mu\mu} + \frac{E^{\frac{1}{2}}}{S}\tilde{p}_{zz}\right) = \left(\tilde{p}_{\mu\mu} + \frac{E^{\frac{1}{2}}}{\sigma S}\tilde{p}_{zz}\right)_{\mu\mu},$$

subject to the boundary conditions

$$\frac{2\sigma\epsilon}{r_0 E^{\frac{1}{2}}} J(\tilde{p}, \tilde{p}_z) + \frac{\sigma S}{E^{\frac{1}{2}}}\tilde{p}_{\mu\mu} = \tilde{p}_{z\mu\mu} \quad \text{on } z = 0,$$

$$\frac{2\sigma\epsilon}{r_0 E^{\frac{1}{2}}} J(\tilde{p}, \tilde{p}_z) - \frac{\sigma S}{E^{\frac{1}{2}}}\tilde{p}_{\mu\mu} = \tilde{p}_{z\mu\mu} \quad \text{on } z = 1,$$

$$\tilde{p} = \tilde{p}_\mu = 0 \quad \text{on } \mu = 0,$$

$$\tilde{p}_\mu = -2[a + b(z - \tfrac{1}{2})] \sin\theta, \quad \tilde{p}_{\mu\mu} + \frac{E^{\frac{1}{2}}}{S}\tilde{p}_{zz} = 0 \quad \text{as } \mu \to \infty,$$

where the notation of §3 is used.

This research has been sponsored in part by the Air Force Office of Scientific Research, under Grant AFOSR-83-0069.

REFERENCES

Barcilon, V. & Pedlosky, J. 1967*a* Linear theory of rotating stratified fluid motions. *J. Fluid Mech.* **29**, 1–16.

Barcilon, V. & Pedlosky, J. 1967*b* A unified linear theory of homogeneous and stratified rotating fluids. *J. Fluid Mech.* **29**, 609–621.

Boyer, D. L. 1970 Flow past a right circular cylinder in a rotating frame. *Trans. ASME* D: *J. Basic Engng* **92**, 430–436.

Boyer, D. L. & Davies, P. A. 1982 Flow past a circular cylinder on a β-plane. *Phil. Trans. R. Soc. Lond.* A **306**, 533–556.

Boyer, D. L., Davies, P. A. & Biolley, F. 1984 Linear stratified rotating flow past topography. Presented at the 10th Annual Meeting of the European Geophysical Society, Louvain-la-Neuve, Belgium, 30 July–3 August.

Brevdo, L. & Merkine, L. 1985 Boundary layer separation of a two-layer rotating flow on an f-plane. *Proc. R. Soc. Lond.* A (in press).

Greenspan, H. P. 1968 *The Theory of Rotating Fluids.* Cambridge University Press.

Merkine, L. 1980 Flow separation on a beta plane. *J. Fluid Mech.* **99**, 399–409.

Merkine, L. & Solan, A. 1979 The separation of flow past a cylinder in a rotating system. *J. Fluid Mech.* **92**, 381–392.

Walker, J. D. & Stewartson, K. 1972 The flow past a circular cylinder in a rotating frame. *Z. angew Math. Phys.* **23**, 745–752.